Int. J. Heat Mass Transfer. Vol. 24, No. 7, pp. 1139–1150, 1981
Printed in Great Britain

0017–9310/81/071139–12 $02.00/0
Pergamon Press Ltd.

OPTICAL TOMOGRAPHY FOR FLOW FIELD DIAGNOSTICS

R. J. SANTORO and H. G. SEMERJIAN
Thermal Processes Division, National Bureau of Standards, Washington, D.C., U.S.A.

and

P. J. EMMERMAN and R. GOULARD
School of Engineering and Applied Science, The George Washington University, Washington, D.C., U.S.A.

(*Received* 16 *December* 1980 *and in revised form* 14 *January* 1981)

Abstract — Optical tomography has been applied to an off-axis turbulent methane–air free jet to determine the mean methane concentration throughout the mixing region. Optical tomography is a multi-angular absorption technique which involves making M line of sight absorption measurements (projections) at N angles. These $M \times N$ measurements are then used to reconstruct the original two-dimensional flow field. Absorption measurements were made on methane using the near resonance 3.39 μm line of a He–Ne laser. Mean concentration measurements were obtained at three positions downstream of the jet exit plane. Comparisons with the results of previous workers for the axial and radial mean concentration profiles show good agreement. Additionally, the sensitivity of the reconstructed results to the number of angles and scans used is briefly described. The results demonstrate the unique capabilities of optical tomography for flow field diagnostics.

NOMENCLATURE

a, spacing between parallel beams (spatial interval);
d, inner diameter of the jet orifice;
$F(x, y)$, the property field ($N_i Q_{vi}$);
I_{v0}, incident intensity at frequency v;
I_v, transmitted intensity at frequency v;
k_1, k_2, constants;
M, the number of parallel rays for each projection;
N, the number of projections (viewing angles);
$\bar{N}_i$, the mean concentration of species i;
$\bar{N}_{ic}$, the mean concentration at the centerline;
N_i, the concentration of species i;
N_{i0}, the initial concentration at the jet orifice;
$P(r, \theta)$, the projection at angle θ;
Q_{vi}, the absorption coefficient of species i at wavelength v;
R, the radius of the measurement field;
r, the radial coordinate;
$r_{1/2}$, the radial coordinate at which the mean concentration has reached one-half its centerline value;
s, the path length over which the absorption is measured;
z, the axial coordinate;
z_0, virtual origin of the jet.

Greek symbols

θ, the viewing angle of the projection;
η, $r/(z + z_0)$;
ρ, the spatial frequency in the transform domain;
ρ_{max}, the spatial bandlimit of $P(\omega, \theta)$;
v, the frequency of the intensity source;
ω, $2\pi\rho$.

Superscript

$\hat{}$, indicates Fourier transform operation.

1. INTRODUCTION

FLOW FIELDS typically encountered in combusting and other high temperature reacting flows are spatially and temporally variant and quite complex. Flow characteristics are controlled by nonlinear interactions between chemical and fluid dynamical processes. The characterization of such complex flow fields requires measurements with high spatial and temporal resolution. Recognition of this need has resulted in a considerable effort towards development of a wide range of diagnostic techniques. Of particular significance have been developments in laser-based diagnostics which are now widely used to measure velocity, concentration and temperature.

Techniques which provide point measurements, such as laser scattering, CARS and fluorescence, have received most of the attention, due to their capability to resolve spatially non-homogeneous flows. Absorption diagnostics provide the capability for measuring low concentrations of chemical species, and have been used extensively in analytical instrumentation. However, application of absorption measurements in reacting and fluctuating flows has been limited, due to the path-integrating nature of the measurement and the resultant inability to resolve a non-uniform property field. An 'onion peeling' technique involving

Abel inversion has been used to overcome the path integration limitation of absorption measurements. However, this technique is limited to flow fields with suitable symmetry properties; in addition, 'onion peeling' methods amplify experimental errors [1, 2].

The purpose of this paper is to discuss a multiangular scanning technique (optical tomography) which extends the application of absorption diagnostics to nonuniform flow fields. Multiangular scanning techniques have been successfully applied to medical X-ray tomography [3, 4], radio astronomy [5], interferometry [6] and materials inspection [7, 8]. In addition, extension of this approach for concentration and temperature measurements in combusting flows has been examined [2, 9]. Applications intended for monitoring of atmospheric pollutants have also been proposed [10, 11]. Recent experimental work [9, 12] has established more clearly the constraints and requirements of multiangular absorption techniques for flow diagnostics, and has provided preliminary results demonstrating the feasibility of the approach.

This paper includes results, obtained using the multiangular absorption technique, on a turbulent round jet issuing into a quiescent environment. Comparisons of axial decay rates with the results of previous workers are presented, along with the two-dimensional radial concentration profiles. An examination of the criterion for proper spatial sampling of a bandlimited function is reviewed and compared with the present experimental cases. In addition, the requirements for proper sampling are explicitly compared to simulated test cases previously studied [9, 13].

2. MULTIANGULAR SCANNING

The multiangular absorption technique involves the measurement of absorption along M equally spaced parallel beams at N equally spaced angles, forming an $M \times N$ data set from which it is possible to retrieve or 'reconstruct' the original property field. The absorption along each individual beam is governed by the Bouguer–Lambert–Beer law which can be expressed as

$$I_\nu/I_{\nu 0} = \exp\left(-\int N_i Q_{\nu i}\,\mathrm{d}s\right) \tag{1}$$

where $I_\nu/I_{\nu 0}$ is the ratio of the transmitted to initial intensity at frequency ν, N_i is the concentration of species i which absorbs at frequency ν, $Q_{\nu i}$ is the absorption cross section for N_i at frequency ν, and s is the path length. This equation may be rewritten as (see Fig. 1)

$$-\ln\frac{I_\nu(r,\theta)}{I_{\nu 0}} = P(r,\theta) = \int_{-\infty}^{+\infty} F(x,y)\,\mathrm{d}s \tag{2}$$

where $r = x\cos\theta + y\sin\theta$, $s = -x\sin\theta + y\cos\theta$.

$P(r,\theta)$ is defined as the 'projection' for the angle θ. Since the ratio $I_\nu/I_{\nu 0}$ can be measured experimentally, $P(r,\theta)$ is known and the solution of equation (2) for

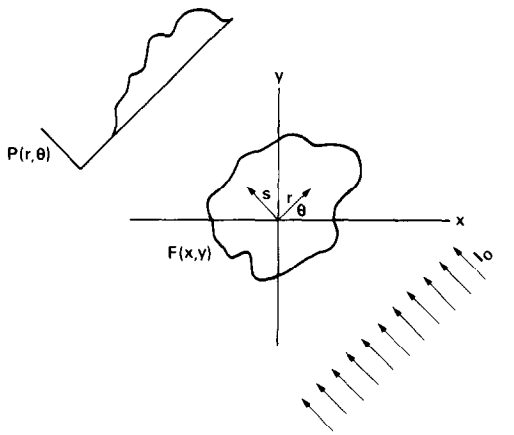

FIG. 1. Projection $P(r,\theta)$ in polar coordinates.

$F(x,y)$ will yield the desired property field $(N_i Q_{\nu i})$. Thus the multiangular scanning technique is based upon the reconstruction of a property field, $F(x,y)$, from a set of its projections, $P(r,\theta)$. Details of the solution procedure have been presented previously [9, 13], and only a brief exposition of the analysis will be given here.

The solution procedure utilizes the convolution technique developed by Ramachandran and Lakshminarayanan [14]. Although it is a Fourier transform approach, this technique does not actually require the evaluation of any transforms, and allows high speed computation of the property field.

In this method the Fourier transform of equation (2) is written

$$\hat{P}(\omega,\theta) = \int_{-\infty}^{+\infty} P(r,\theta)\mathrm{e}^{-i\omega r}\,\mathrm{d}r = \int_{-\infty}^{+\infty}\int_{-\infty}^{+\infty} F(r,s)\,\mathrm{e}^{-i\omega r}\,\mathrm{d}r\,\mathrm{d}s \tag{3}$$

where $\omega = 2\pi\rho$ and ρ is the spatial frequency. The Fourier transform of $P(r,\theta)$ can be related to the two-dimensional Fourier transform of $F(r,s)$

$$\hat{F}(\omega,\theta) \equiv \int_{-\infty}^{+\infty}\int_{-\infty}^{+\infty} F(r,s)\mathrm{e}^{-i(\omega r+\eta s)}\,\mathrm{d}r\,\mathrm{d}s\big|_{\eta=0} \tag{4}$$

when it is evaluated along the line $\eta = 0$ in the two-dimensional frequency plane. This is the 'central slice theorem' (see e.g. [4]) which relates the one-dimensional Fourier transform ($\eta = 0$) of the one-dimensional projection $P(r,\theta)$ to the two-dimensional Fourier transform of the property field $F(r,s)$. This theorem expresses the fact that the one-dimensional Fourier transform of the projection is a 'slice' through the Fourier transform plane of $F(r,s)$ at the angle θ (see Fig. 2). For each value of θ, the values of $\hat{F}(\omega,\theta)$ can be plotted for all pertinent values of ω. A 180° sweep of θ yields all values of $\hat{F}(\omega,\theta)$ in the Fourier transform plane. The function $F(x,y)$ can therefore be retrieved as the inverse Fourier transform of the set of $\hat{P}(\omega,\theta)$ which are derived from the experimentally measured projections.

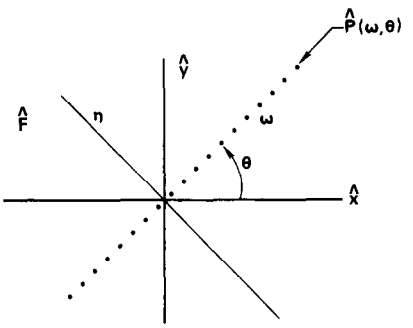

FIG. 2. The central slice theorem.

If equation (4) is expressed in Cartesian coordinates and the inverse transform operation is performed, then $F(x, y)$ is given by

$$F(x,y) = \frac{1}{4\pi^2}\int_0^{\pi} d\theta \int_{-\infty}^{+\infty} \hat{P}(\omega,\theta)\, e^{i\omega(x\cos\theta + y\sin\theta)} |\omega|\, d\omega \tag{5}$$

Now let V be equal to the inner integral

$$V(r,\theta) = \frac{1}{2\pi}\int_{-\infty}^{+\infty} \hat{P}(\omega,\theta)|\omega| e^{i\omega r} d\omega$$

and define a function ϕ such that its Fourier transform is given as

$$\hat{\phi}(\omega) = |\omega|.$$

Then from the convolution theorem for Fourier transforms

$$V(r,\theta) = \int_{-\infty}^{+\infty} P(\tau,\theta)\,\phi(r-\tau)\,d\tau \tag{6}$$

and

$$F(x,y) = \frac{1}{2\pi}\int_0^{\pi} d\theta \int_{-\infty}^{+\infty} P(\tau,\theta)$$

$$\phi(x\cos\theta + y\sin\theta - \tau)d\tau. \tag{7}$$

Since $P(r, \theta)$ is known only in the sampled domain, the integrals in equation (7) must be replaced by their discrete summation approximations. Thus,

$$F(x,y) = \frac{a}{2N}\sum_{j=1}^{N}\sum_{k=1}^{M} P(r_k,\theta_j)\phi(x\cos\theta_j + y\sin\theta_j - r_k) \tag{8}$$

where a is the spacing between uniform samples and

$$\theta_j = (j-1)\pi/N \quad r_k = ka.$$

ϕ may be interpreted as a weighting function of the distance from the point (x, y), where the property $F(x, y)$ is to be evaluated, to r_k where a value of the projection $P(r, \theta)$ is evaluated. An accurate reconstruction will require that the Fourier transform of ϕ satisfies the condition $\hat{\phi}(\omega) \cong |\omega| < 2\pi\rho_{max}$, where ρ_{max} is the radius of the transform space. The choice of the function $\phi(r)$ greatly affects the computational requirements as well as the accuracy of the results. In the present study the modified Shepp–Logan filter [15] has been used

$$\bar{\phi}(r_k) = 0.4\phi(r_k) + 0.3\phi(r_{k+1}) + 0.3\phi(r_{k-1}) \tag{9}$$

$$\phi(r_k) = -\frac{4}{\pi a^2(4k^2-1)} \quad k = 0, \pm 1, \pm 2, \ldots$$

$\phi(r)$ can be considered a filter function (see Kwoh, Reed and Truoung [16] for a comparison of various filter functions) and its selection must be dependent on the noise of the instrumentation system as well as the bandlimit of the function (see Section 5).

Accurate reconstruction of the property field, $N_i Q_{vi}$, will be dependent on the proper choice of the sampling intervals, that is the choice of M and N, as well as the choice of the appropriate form of the filter function, ϕ.

From the sampling theorem [17], a function can be uniquely recovered from its samples if it is sampled at a rate greater than twice the highest frequency component of the function (sampling rate $\geq 2\rho_{max}$). The present function, $F(x, y)$, is assumed to have a band-limited Fourier transform, i.e. $\hat{F}(x, y) \equiv \hat{F}_\theta(\rho) = 0$ for $\rho > \rho_{max}$, while in the measurement or physical space $F(x, y) = 0$ if $r = x^2 + y^2 \geq R$, where R is the radius of the measurement space. The proper choice of M and N under these conditions, which has been discussed previously [9], requires that $(4R\rho_{max})$ equally spaced rays are measured at $(2\pi R\rho_{max})$ equally spaced angles. If this criterion is not met, the reconstructed field is likely to show effects due to 'aliasing' [18]. Aliasing is a term used to describe the effects observed when a function is undersampled. In such a case the sampled function contains contributions from the undersampled high frequency components which appear as lower frequency contributions in the transform domain. Unambiguous identification of aliasing effects requires a knowledge of the original function from which accurate comparisons can be made. Operationally one could increase the sample rate until aliasing effects are observed to be unimportant. Once these minimum sampling conditions have been satisfied, additional higher frequency sampling (i.e. oversampling) although unnecessary from a theoretical viewpoint, in general can improve the reconstruction in the presence of noise.

3. EXPERIMENTAL

The objective of the present experimental program is to provide a preliminary assessment of the utility of multiangular absorption techniques for combustion diagnostics. In order to minimize experimental difficulties introduced by combustion, a simple flow con-

figuration has been chosen for these initial experiments. A turbulent methane–air diffusion jet expanding into ambient air has been studied under steady flow conditions, at atmospheric pressure and room temperature. The jet apparatus consists of a 10.8 mm I.D. brass tube located 19 mm from the center line of a 15.25 cm dia. brass plate. Locating the jet off the centerline introduces an apparent asymmetry into the flow upon rotation of the circular plate. The jet flow is supplied from a 10 cm dia. cylindrical chamber containing a mixing section filled with glass beads. Flow straighteners and screens are contained in the jet section to provide a relatively uniform exit flow profile. The jet/plane combination is mounted on a milling machine bed which allows for accurate three-dimensional positioning of the unit. The precision of positioning was limited by the resolution of the milling machine bed which was 0.025 mm. However, the apparatus centerline could only be determined with an accuracy of ± 0.25 mm.

Mixtures of 10% methane–90% air were used in all experiments. Matheson* technical grade methane and air supplied from an in-house compressor were used. All flows were monitored using rotameters. The jet exit flow conditions corresponded to a Reynolds number of 29 000 and an exit velocity of 35 m s^{-1}.

Concentration measurements were based on absorption by methane of the near resonant 3.39 μm line of a He–Ne laser [19]. The experimental arrangement for the absorption measurements is shown in Fig. 3. A Spectra Physics Model 120 He–Ne laser operating at 3.39 μm with an output of approximately 2 mW was used as the laser light source. A quartz lens with a 20 cm focal length was used to produce a beam whose diameter across the jet/plate region was 1.3 mm. A second 20 cm lens then focused the transmitted beam on a radiometer (Laser Precision Model RK 5100). This unit utilizes a pyroelectric detector and lock-in amplifier detection to monitor the laser intensity and provides a convenient means of measuring the full laser intensity with suitable thermal stability and background noise rejection. The output of the lock-in amplifier was monitored with Fluke Model 2240B Datalogger, and the digital data were transferred to a DEC PDP 11/60 minicomputer for storage.

A complete set of absorption measurements was made across the jet at three axial locations, $z = 1.27$, 12.7 and 25.4 cm downstream of the jet exit plane. At each axial location, projections were obtained for 12 separate angles. At each angle, the projection was determined by incrementally traversing the jet through the laser beam. The jet was then rotated 15° and the

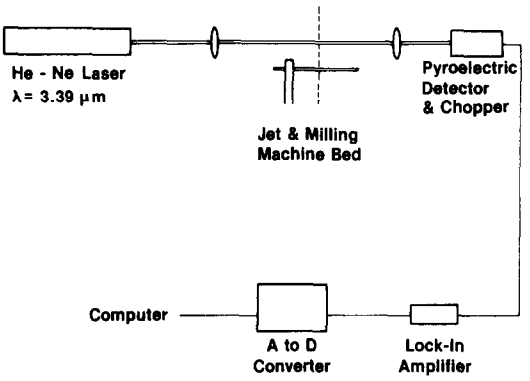

FIG. 3. Schematic of experimental apparatus.

measurements were repeated. The parallel beam spacing for each axial location was chosen to keep the number of absorption measurements within the jet nearly constant. Therefore the spatial sampling interval was increased at larger axial distances. This resulted in a radial span of 6.4 cm (101 points) at $z = 1.27$ cm, 10.2 cm (81 points) at $z = 12.7$ cm, and 20.4 cm (81 points) at $z = 25.4$ cm. For each parallel ray, 50 readings were taken and the average value was used in all further calculations. For the present experiments the detection system was operated with a 0.1 s time constant, and individual intensity readings were taken at 0.2 s intervals.

The axial locations for the measurements were chosen to span the characteristic regions of the flow and thus present a variety of measurement conditions. In particular, the near exit location ($z = 1.27$ cm) should exhibit the steepest gradients and thus be more susceptible to aliasing effects. The $z = 25.4$ cm position should be in the similarity region of the flow and thus provides the best conditions for comparisons with the results of previous workers. The $z = 12.7$ cm location provides a position where an estimate of the location of transition to the similarity region can be made.

4. RESULTS

The projection data were analyzed as described previously in Section 2, and a reconstruction of the concentration profile at each axial position was obtained using equation (8). The reconstruction results are shown in Figs. 4–6. These plots of the concentration profiles are given as the product $N_t Q_{vi}$ since it is this quantity which is actually obtained from the analysis. The concentration of methane can be found by dividing the linear absorption coefficient, $N_t Q_{vi}$, by the absorption coefficient for methane. For the present experimental conditions the results of McMahon *et al.* [19] have been extrapolated to yield a value of 10 atm^{-1} cm^{-1} for Q_{vi}. It must be emphasized that since the projections were taken in a sequential manner as previously described, these profiles represent the time averaged (mean) values of the linear absorption coefficient in the jet.

*Certain commercial equipment, instruments, or materials are identified in this paper in order to adequately specify the experimental procedure. In no case does such identification imply recommendation or endorsement by the National Bureau of Standards, nor does it imply that the material or equipment identified is necessarily the best available for the purpose.

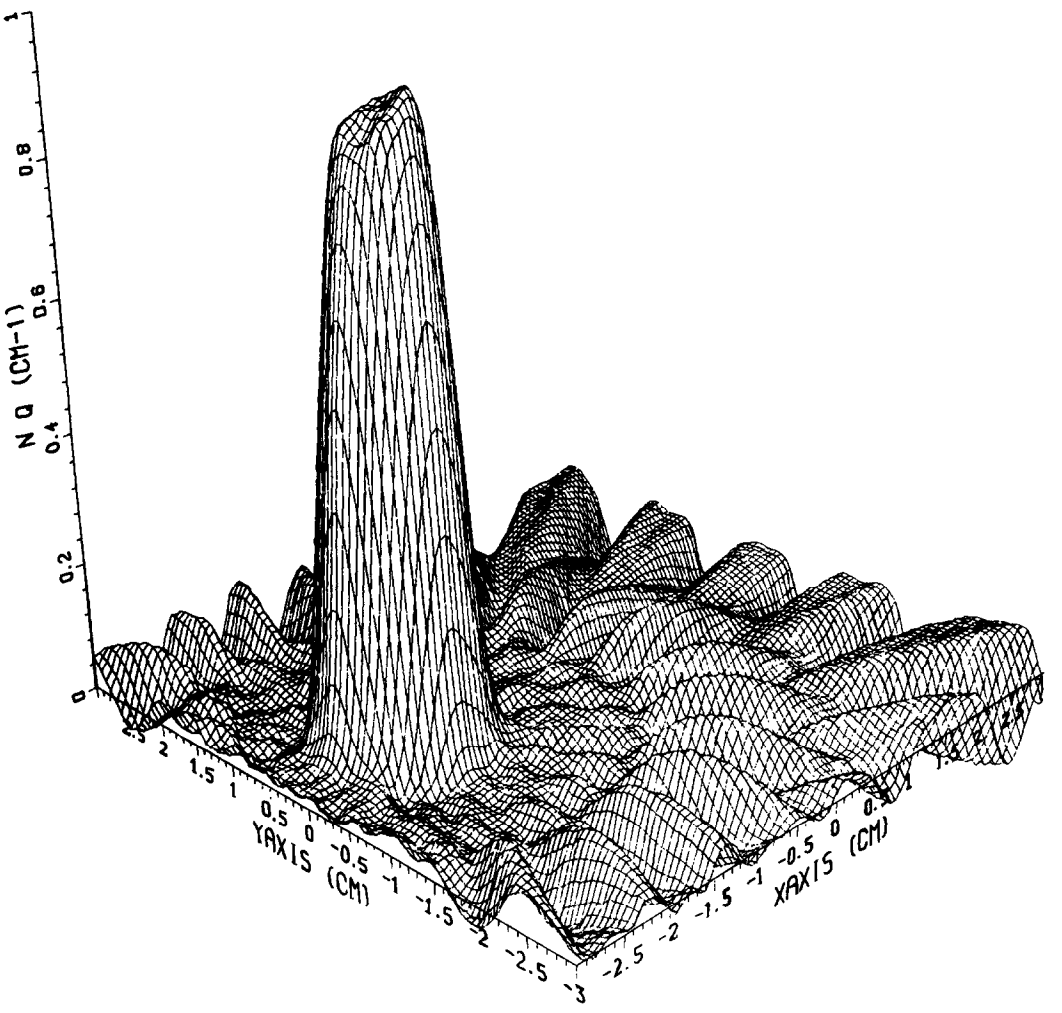

FIG. 4. Reconstructed property field $N_i Q_{vi}$ for $z = 1.27$ cm.

The concentration profiles show qualitatively the features one expects. Close to the jet the profile has a top-hat character while as the axial distance increases a more Gaussian profile is observed. These profiles show a smooth expansion between the $z = 12.7$ and $z = 25.4$ cm positions. It should be noted that Figs. 4–6 are plotted with different scales while the figure size is maintained constant for readability. In general the reconstructions appear satisfactorily devoid of noise and aliasing effects. This is somewhat less true for the $z = 1.27$ cm axial position where some aliasing, particularly at the boundary of the spatial domain, is noted. This effect is due to the sharp concentration gradients present which require high spatial sampling for proper reconstruction. In addition to the aliasing away from the jet, the peak values do show a 10% variation across the top-hat portion of the profile. This is likely to be due to aliasing. Further discussion of the importance of aliasing, noise and filtering will be presented later in this paper.

Quantitative comparisons have been made to assess the internal consistency of the data as well as to compare with previous results on similar jets. Since the jet/plate arrangement introduced an asymmetry upon rotation, the position of the jet centerline presented a test for the multiangular absorption technique. The centroid position for each of the profiles was calculated from the linear absorption coefficient values and found to be 18.5, 19.8 and 19.3 mm respectively for the three axial positions. These compare well with the known jet position of 19 mm from the centerline of the plate. As a check on the concentration measurements, a comparison between the concentration value at the $z = 1.27$ cm position and the measured flow was made assuming the absorption coefficient to be $10\,\text{atm}^{-1}\,\text{cm}^{-1}$. At this position the concentration within the potential core has not decayed from its initial value. The methane concentration obtained from the absorption measurements was 9% compared to the rotameter measurement of 10% methane. Considering the uncertainties in the rotameter measurements (±5%) and the extrapolated value for the absorption coefficient, this agreement is satisfactory.

To verify the consistency of the reconstruction results with the original data, the reconstructed con-

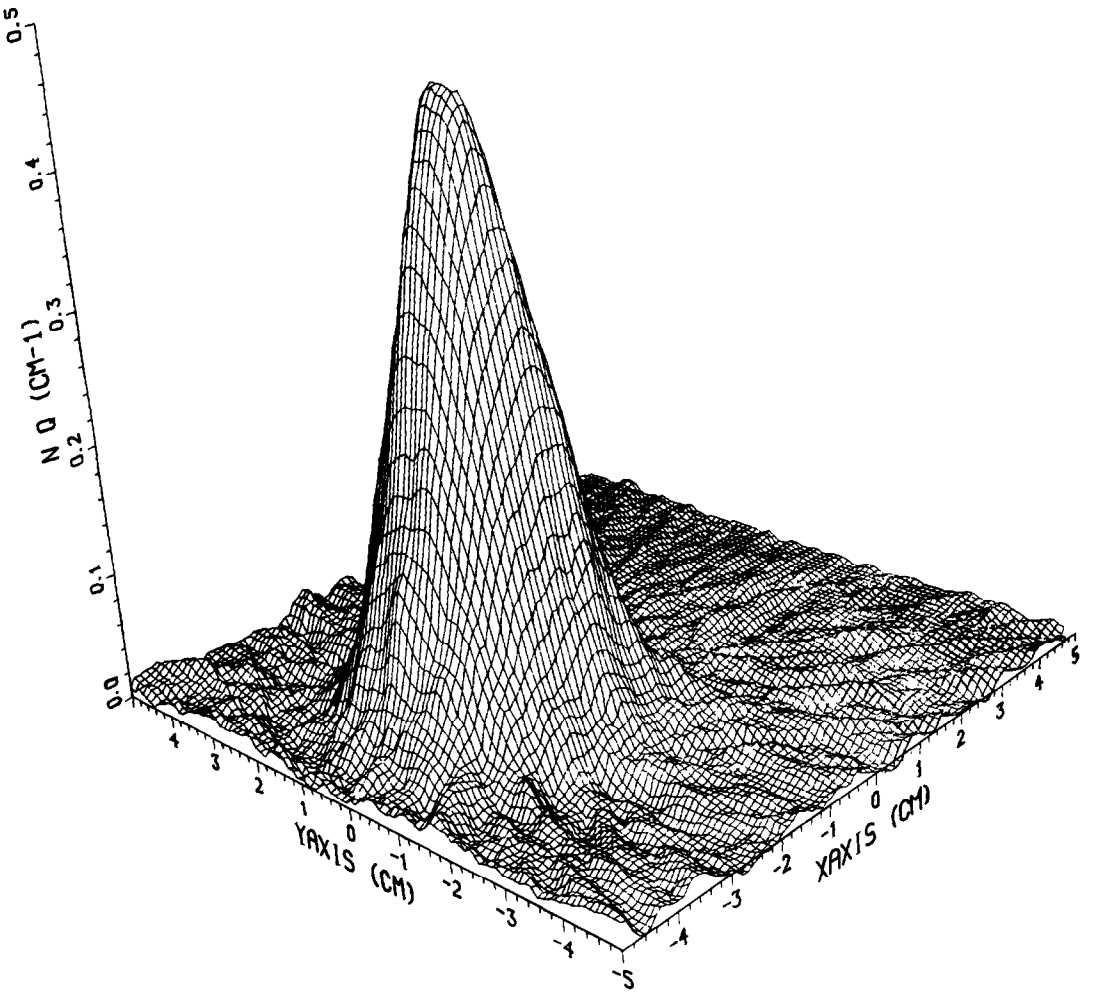

FIG. 5. Reconstructed property field $N_i Q_{vi}$ for $z = 12.7$ cm.

centration profiles were integrated for comparison with the original projections, (see Fig. 7). Agreement is excellent for the $z = 12.7$ and $z = 25.4$ cm positions with some differences observed for the $z = 1.27$ cm position. For this latter case the error observed is traceable to the increased aliasing observed at this position as discussed earlier.

Measurements of the mean concentration in a free turbulent jet discharging into a stagnant atmosphere have been presented by several workers [20–23]. These studies have involved point measurement techniques such as Raman scattering [20], laser particle scattering [21, 22] and sampling probes [23], and include extensive investigations of both the mean and fluctuating characteristics of such jets. For the present study comparisons are limited to the mean concentration results.

The decay of the normalized mean concentration along the centerline is usually expressed [20] as

$$\bar{N}_{ic}/N_{i0} = k_1 d/(z + z_0) \qquad (10)$$

where $\bar{N}_{ic}/N_{i0}$ is the ratio of the mean centerline concentration at the axial location z, divided by the initial concentration, d is the jet diameter, and k_1 and z_0 are constants. Previous workers have reported results in the form of equation (10) typically for values of z/d equal or greater than 20. For positions where z is less than 20 jet diameters, the flow does not exhibit sufficient similarity for equation (10) to be appropriate. Table 1 shows the comparison of the results for $z/d \geq 20$ from studies by Becker, Hottel and Williams [22], Birch *et al.* [20], and Hinze and Van der Hegge Zijnen [23] with those of $z = 25.4$ cm for the present case. For $z = 12.7$ cm the plotted data from [22] are shown along with the results of [23]. Agreement with previous studies is considered good. Because of the limited number of axial stations examined, no attempt has been made to express the present results in the form of equation (10). The ratios given in Table 1 for this work were obtained using the value for $N_i Q_{vi}$ obtained for $z = 1.27$ cm position for the initial concentration. The concentration at this point has not decayed from the exit plane value, and its use eliminates the need for choosing a value for Q_{vi}.

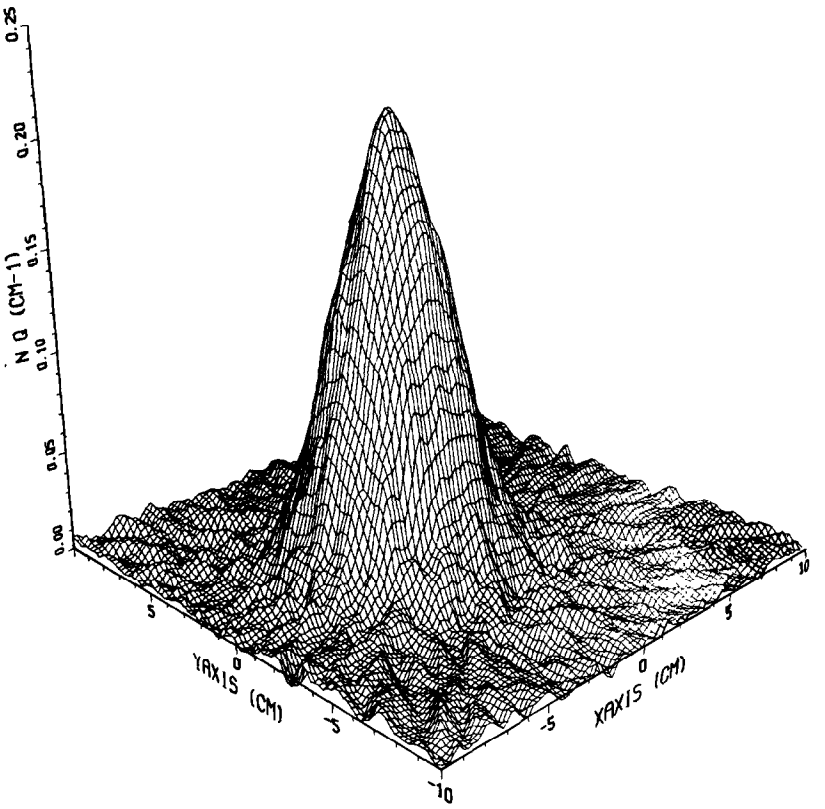

FIG. 6. Reconstructed property field $N_i Q_{vi}$ for $z = 25.4$ cm.

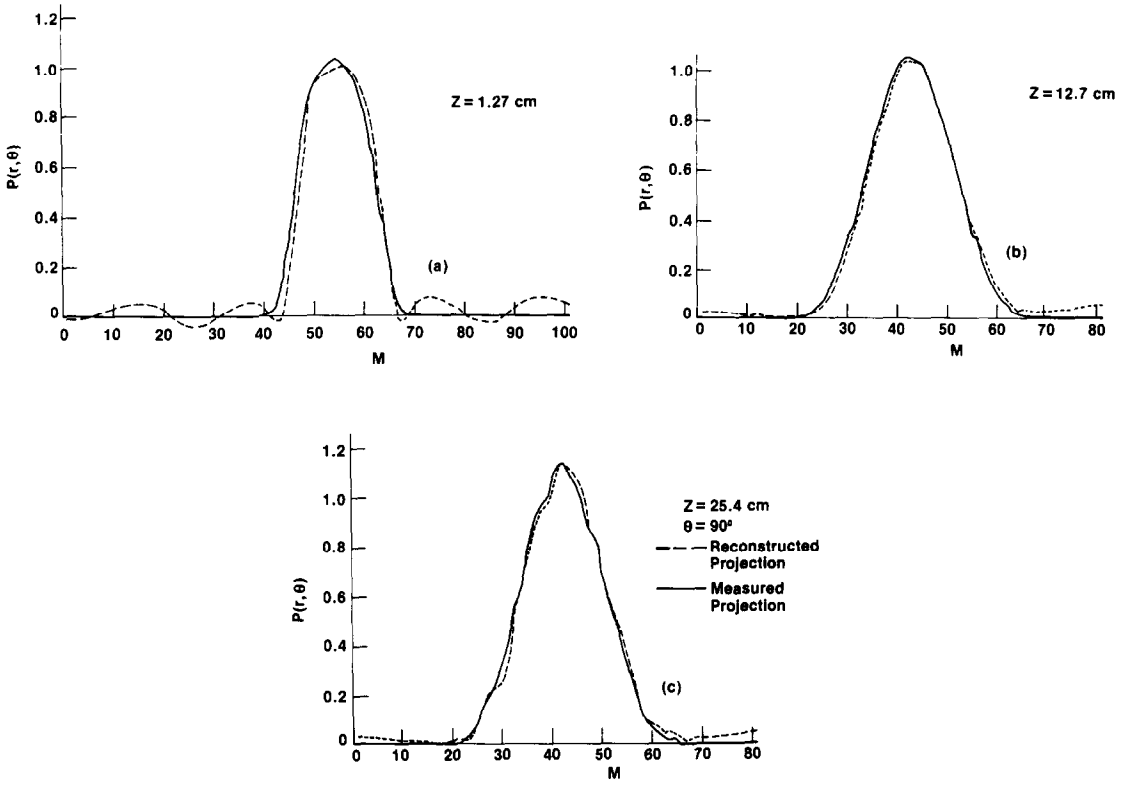

FIG. 7. Comparison of reconstructed projections with measured projections: (a) $z = 1.27$ cm, (b) $z = 12.7$ cm, (c) $z = 25.4$ cm; —— measured projection; – – – reconstructed projection.

Table 1. Comparison of the normalized axial mean concentration

Z (cm)	Z/d	Becker [22]	Birch [20]	Hinze [23]	This paper
12.7	11.8	0.53*	—	0.42	0.50
25.4	23.5	0.26	0.22	0.22	0.24

*Taken from plot of data.

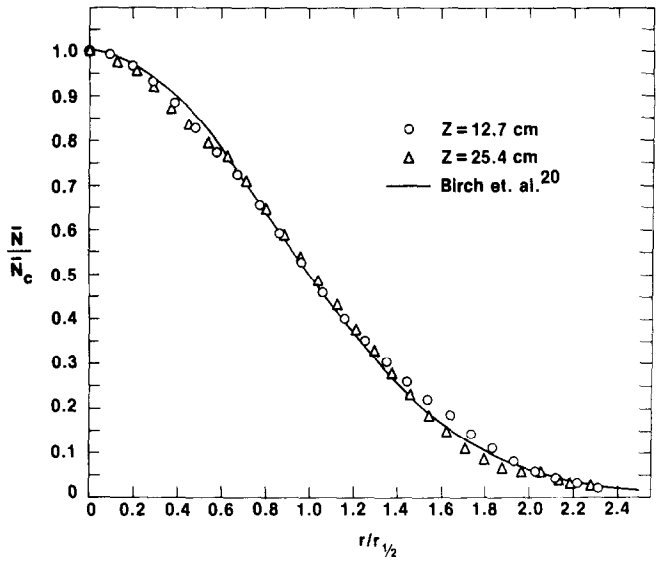

FIG. 8. Normalized radial concentration as a function of $r/r_{1/2}$.

Figure 8 shows the results for the radial profile of the normalized mean concentration for the axial positions 12.7 and 25.4 cm as a function of $r/r_{1/2}$ where $r_{1/2}$ is the position at which the mean concentration has reached one-half of its centerline value. Similarity of the profiles for these positions is clear, and agreement with the results of Birch *et al.* [20] is very good. The data were also fit to a self-preserving form given by Becker, Hottel and Williams [22]

$$\bar{N}_i/\bar{N}_{ic} = \exp(-k_2\eta^2) \tag{11}$$

with $\eta = r/(z + z_0)$. Our results along with the results

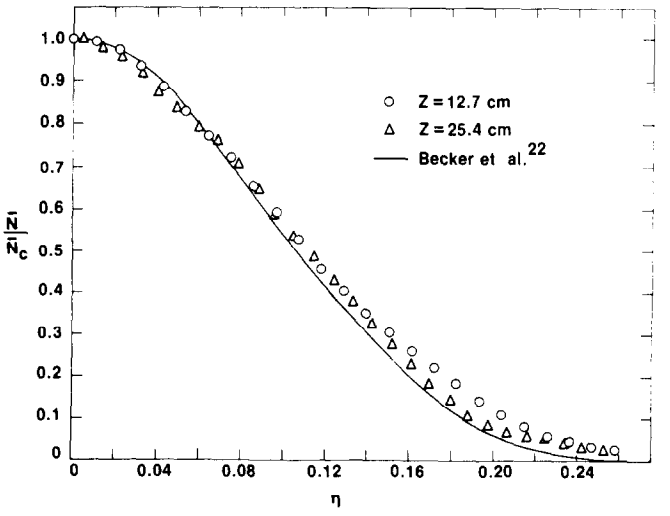

FIG. 9. Normalized radial concentration as a function of $\eta = r/(z + z_0)$.

Table 2. Comparison of the normalized jet half-width ($r_{1/2}/d$)

Z (cm)	Z/d	Becker [22]	Birch [20]	Shaughnessy [21]	This paper
12.7	11.8	1.14 (0.99)*	1.14	—	0.98
25.4	23.5	2.24	2.28	2.38	2.28

*Obtained from equation (1) of [22].

of Becker, Hottel and Williams ($k_2 = 61.6$ and $z_0 = -2.4d$) are shown in Fig. 9. A least squares fit to our data for $z = 25.4$ cm yields values of $k_2 = 62.0$ and $z_0 = -3.0d$. Again very good agreement is obtained with the results of Becker, Hottel and Williams.

Table 2 presents a comparison of the results of previous measurements of $r_{1/2}/d$ with our results Agreement at the $z = 25.4$ cm location is excellent. The axial location at which similarity is attained varies from 8 to 20 diameters and is probably a function of the jet configuration and initial flow conditions. At the $z = 12.7$ cm location, the agreement with the data of Birch and Becker and their co-workers is not as good if it is assumed that the jet is not fully developed. However, the results shown in Fig. 8 indicate that the flow is already fully developed at $z = 12.7$ cm. Based on this observation, if the measured jet half-width is compared to the value obtained from the analytical expression of Becker for the similarity region ($r_{1/2}/d = 0.99$), then the agreement is quite good.

The agreement shown for the axial and radial mean concentration clearly establishes that the multiangular absorption approach can provide accurate measurement of the time-averaged properties of the flow field. Similar comparison for fluctuating quantities will require a more involved instrumentation approach and will be discussed in the next section.

As a final comparison, the property field for a single axial location ($z = 12.7$ cm) was reconstructed using the data from only six angles, with the objective of providing a point of comparison with previous multiangular scanning simulation studies [9, 13]. The results for the six-angle case are shown in Fig. 10. The increase in aliasing effects at the edges of the reconstruction can be easily seen, although the jet region itself shows very little difference from the full twelve angle case shown in Fig. 5.

The previous results using simulated 'noiseless' test functions [9] are shown in Fig. 11. The effect of decreasing the number of projections (i.e. the number of angles used) resulted in an increase in the aliasing effects observed in the reconstructed function. A comparison of the $N = 6$ and $N = 10$ of Fig. 11 with Figs. 10 and 5, respectively shows that the simulated test function studies quite accurately represent the effects observed for this experimental work.

5. DISCUSSION

Reconstruction errors

Part of the motivation for obtaining concentration measurements at various axial locations was to evaluate the effect of increasing the bandlimit of the sampled concentration property field. The bandlimit of a function refers to the highest frequency component present in the transformed function. The spatial intervals a and $\Delta\theta$ must be chosen such that the corresponding spatial frequencies $1/a$ and $1/R\Delta\theta$ (which determine the highest sampling frequencies) satisfy the requirements of the sampling theorem for the function (see Section 2). The highest bandlimit occurred for the near-exit position of $z = 1.27$ cm, where the concentration gradients were the steepest, and the lowest bandlimit occurred at $z = 25.4$ cm. Quantitative information concerning the bandlimit was obtained by taking the discrete Fourier transform of the input projection data and choosing the bandlimit to be the frequency at which 99% of the energy spectrum was included. The energy spectrum is chosen since, from Parseval's formula [17], we know the energy to be conserved in transforming from the spatial to the frequency domain. The Fourier analysis [24] yields bandlimits of 0.94, 0.4 and 0.2 cm^{-1} for the 1.27, 12.7 and 25.4 cm axial positions, respectively. According to the results presented in Section 2 for the present values for M and N, the angular and parallel ray sampling limits which satisfy the sampling theorem condition are 0.6 and 8.0 cm^{-1}, 0.4 and 4.0 cm^{-1},

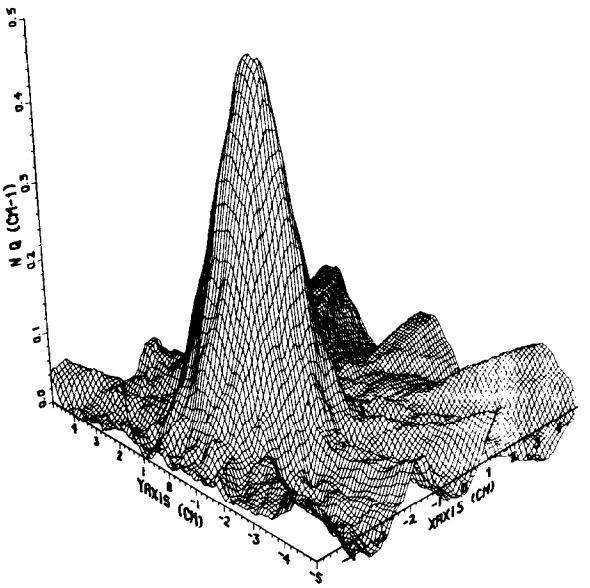

FIG. 10. Reconstructed property field $N_i Q_{vi}$ for $z = 12.7$ cm using six projections (viewing angles).

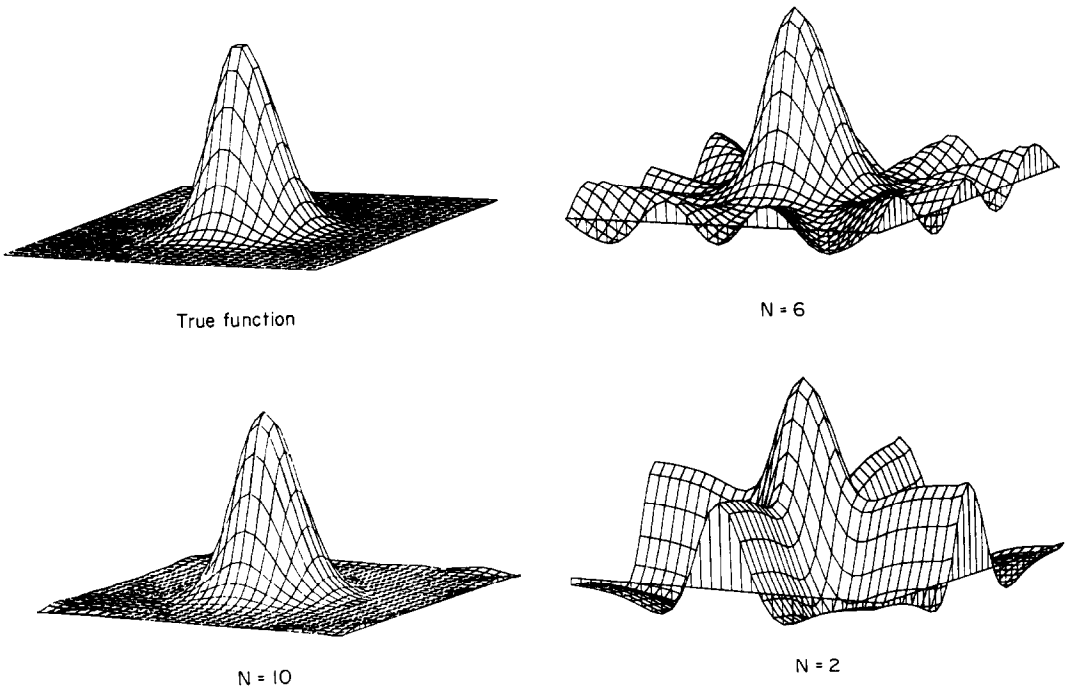

FIG. 11. Reconstruction of a Gaussian function using N projections (viewing angles).

and 0.2 and 1.99 cm^{-1}, respectively as the axial location increases. Therefore, we see that in terms of the parallel rays the property field is oversampled while the angular requirement is adequately met for the 12.7 and 25.4 cm locations, but is undersampled for the 1.27 cm location. In fact, based on the bandlimit, previous analysis predicts that 18 angles rather than 12 are required for adequate sampling of the field near the jet exit plane. The consequences of undersampling are reflected in the observed aliasing effects described in Section 4 for this location. The close agreement between the observed sampling requirements and those calculated based on previous simulation studies [9, 13] is supportive of further extension of the multiangular absorption technique to more complicated flow configurations where simulated results have shown promise.

Noise and filtering

In Section 2 it was pointed out that in order to reconstruct the property field $F(x, y)$, using equation (8), the weighting function $\phi(r)$ must be chosen. Several such functions have been considered in the literature [14–16], and for the present study the modified Shepp–Logan filter [15] has been used. The choice of the weighting function can have a significant effect on the 'noise' observed in the reconstructed property field. Statistical fluctuations due to the light source or detector system are likely sources of noise for real time systems. The requirement that the data be obtained sequentially introduces an additional 'noise' source for the present case. This 'noise' results from the fluctuations in absorptivity and the statistical variation due to the sampling procedure used to obtain the data. The approach to the treatment of noise is therefore closely related to the nature of the experiment and must be addressed as a unique and specific problem.

For this study the discrete Fourier transform analysis provided an estimate of the bandlimit of the projection and thus represented a criterion for comparison with the bandpass of the filter function. The modified Shepp–Logan filter was found to closely approximate $|\omega|$ for frequencies below the bandlimits presented in the previous section while attenuating frequencies outside the bandlimit [24].

Future work

This series of experiments has examined the applicability of multiangular absorption techniques for flow diagnostics. The results have demonstrated that accurate mean concentration measurements can be obtained in situations where asymmetrics are present. For utility as a flow diagnostic technique, however, real time measurements are desirable. Real-time measurements require that all the data be acquired simultaneously, i.e. M absorption measurements must be made at N angles at one instant in time. This requirement can be achieved with the use of presently available photo-array detectors coupled with high speed digital processing. The present results indicate in support of previous work [9] that a modest number of angles are required, while available linear arrays easily meet the parallel ray sampling requirements.

Absorption based diagnostics have the advantage of high sensitivity for a wide variety of species [9, 25]. Multiangular absorption applications can be con-

sidered for measurements in the infrared, visible and near ultraviolet regions of the spectrum. Specific choices are sensitive to the availability and cost of suitable light sources and detector arrays. Additional considerations arise when combusting flows are studied. In future work two major objectives are envisioned: (a) to demonstrate real-time measurement capability; and (b) to examine the complications arising from combustion.

Practical considerations favor the visible and near ultraviolet regions of spectrum, and a silicon photoarray system is being prepared. This system will allow complete property field measurements to be obtained at a 10 kHz rate with aperture times of 50 μs. The maximum measurement rate (10 kHz) is well within the limitations imposed by detector array scan rates, sensitivity and available digital processing rates (e.g. analog to digital conversion and data storage requirement). This rate corresponds to exposure times necessary to 'freeze' the turbulent eddy structure of the jet, as illustrated by high speed (6 kHz) photography studies [26, 27].

Consideration of combustion effects will be investigated from both the mean concentration approaches described in this work and the real-time measurements discussed in this section. Mean concentration measurements in a methane diffusion flame will be used to examine the effect of steep gradients in refractive index, temperature and concentration introduced by combustion. Previous diffusion flame studies [28] have shown that gradients found in flames are similar to those observed in this study. Similar considerations will be investigated in seeded flows with the real-time system.

6. CONCLUSIONS

The multiangular absorption approach has been applied to the measurement of a turbulent jet exiting into a quiescent atmosphere. The technique has been demonstrated to be capable of accurate concentration and position determination in cases without axial symmetry. Comparison of mean concentration profiles with those obtained by previous workers has shown good agreement with the reconstructed property field. Analysis of the importance of appropriate spatial sampling has been presented and compared with previous simulation studies. These comparisons have further validated the accuracy and usefulness of those studies while providing further incentive for the extension of multiangular techniques to more complex flow conditions.

Acknowledgements — The authors with to acknowledge the assistance of J. Abi Samra in running the experiments and aiding with the analysis; I. C. Ball for his help with the three-dimensional plots. Support for two of the authors (P.J.E. and R.G.) was provided from the U.S. Air Force Office of Scientific Research (AF 77-3439) and is gratefully acknowledged.

REFERENCES

1. R. H. Tourin, *Spectroscopic Gas Temperature Measurement*, Chapter 5. Elsevier, New York (1966).
2. F. P. Chen and R. Goulard, Retrieval of arbitrary concentration and temperature fields by multiangular scanning techniques, *J. Quant. Spectrosc. Radiat. Transfer* **16,** 819–827 (1976).
3. R. Gordon, G. T. Herman and S. A. Johnson, Image reconstruction from projections, *Scient. Am.* **233**(4), 56–68 (1975).
4. W. Swindall and H. H. Barrett, Computerized tomography: taking sectional X-rays, *Physics Today* **30**(12), 34–41 (1977).
5. R. N. Bracewell and A. C. Riddle, Inversion of fan-beam scans in radio astronomy, *Astrophys. J.* **150,** 427–434 (1967).
6. D. W. Sweeney and C. M. Vest, Measurement of three dimensional temperature fields above heated surfaces by holographic interferometry, *Int. J. Heat Mass Transfer* **17,** 1443–1454 (1974).
7. J. F. Greenleaf and S. A. Johnson, Algebraic reconstruction of spatial distributions of refractive index and attenuation in tissues from time-of-flight and amplitude profiles, p. 109, in *Ultrasonic Tissue Characterization*, (edited by M. Linzer). NBS Special Publication 453 (1976).
8. R. P. Kruger and T. M. Cannon, The application of computer tomography, boundary detection, and shaded graphics reconstruction to industrial inspection, *Materials Evaluation* **36,** 75–80 (1978).
9. (a) P. J. Emmerman, R. Goulard, R. J. Santoro and H. G. Semerjian, Multiangular absorption diagnostics of a turbulent argon–methane jet, *J. Energy* **4,** 70–77 (1980). (b) R. Goulard and P. J. Emmerman, Absorption Diagnostics, AIAA Paper 79-0085, presented at the AIAA 17th Aerospace Sciences Meeting, New Orleans, LA, Jan. 15–17 (1979).
10. B. W. Stuck, A new proposal for estimating the spatial concentration of certain types of air pollutants, *J. Opt. Soc. Am.* **67,** 668–678 (1977).
11. R. L. Byer and L. A. Shepp, Two-dimensional remote air-pollution monitoring via tomography, *Optics Letters* **4,** 75–77 (1979).
12. R. J. Santoro, H. G. Semerjian, P. J. Emmerman, R. Goulard and R. Shabahang, Multiangular absorption measurements in a methane diffusion jet, p. 427, in *Laser Probes for Combustion Chemistry*, (edited by D. Crosley) ACS Symposium Series 134. American Chemical Society, Washington, D.C. (1980).
13. P. J. Emmerman, Application of tomographic reconstruction to combustion and fluid flow diagnostics. D.Sc. Thesis, George Washington University, Washington, D.C. (1980).
14. G. N. Ramachandran and A. V. Lakshminarayanan, Three-dimensional reconstruction from radiographs and electron micrographs: application of convolutions instead of Fourier transforms, *Proc. Nat. Acad. Sci. U.S.A.* **68,** 2236–2240 (1971).
15. L. A. Shepp and B. F. Logan, The Fourier reconstruction of a head section, *IEEE Trans Nucl. Sci.* **NS-21,** 21–43 (1974).
16. J. S. Kwoh, I. S. Reed and T. K. Truoung, A generalized $|\omega|$ filter for 3-D reconstruction, *IEEE Trans. Nucl. Sci.* **NS-24,** 1990–1998 (1977).
17. S. A. Tretter, *Introduction to Discrete-Time Signal Processing*, p. 14. John Wiley, New York (1976).
18. R. N. Bracewell, *The Fourier Transform and Its Applications*, Chap. 10, 2nd edn. McGraw-Hill, New York (1978).
19. J. McMahon, G. J. Troup, G. Hubbert and T. G. Kyle, The effect of pressure and temperature on the half-width of the methane absorption at 3.39 μm, *J. Quant. Spectrosc. Radiat. Transfer* **12,** 797–805 (1972).

20. A. D. Birch, D. R. Brown, M. G. Dodson and J. R. Thomas, The turbulent concentration field of a methane jet, *J. Fluid Mech.* **88,** 431–449 (1978).
21. E. J. Shaughnessy and J. B. Morton, Laser light-scattering measurements of particle concentration in the turbulent jet, *J. Fluid Mech.* **80,** 129–148 (1977).
22. H. A. Becker, H. C. Hottel and G. C. Williams, The nozzle-fluid concentration field of the round, turbulent, free jet, *J. Fluid Mech.* **30,** 285–303 (1967).
23. J. O. Hinze and B. G. Van der Hegge Zijnen, Transfer of heat and matter in the turbulent mixing zone of an axially symmetrical jet, *Appl. Sci. Res.* **A1,** 435–461 (1949).
24. Unpublished research.
25. C. K. N. Patel, Laser detection of pollution, *Science, N.Y.* **202,** 157–173 (1978).
26. A. R. Ganji and R. F. Sawyer, An experimental study of the flow field and pollutant formation in two-dimensional premixed turbulent flames, AIAA Paper 79-0017, presented at the AIAA 17th Aerospace Sciences Meeting, New Orleans, LA, Jan. 15–17 (1979).
27. N. A. Chigier and A. J. Yule, The physical structure of turbulent flames, AIAA Paper 79-0217, presented at the AIAA 17th Aerospace Sciences Meeting, New Orleans, LA, Jan. 15–17 (1979).
28. R. E. Mitchell, A. F. Sarofim and L. A. Clomburg, Experimental and numerical investigation of confined laminar diffusion flames, *Combust. Flame* **37,** 227–244 (1980).

TOMOGRAPHIE OPTIQUE POUR LE DIAGNOSTIC DES CHAMPS D'ECOULEMENT

Résume—La tomographie optique est appliquée à un jet libre turbulent de méthane et d'air pour déterminer la concentration moyenne du méthane dans la région de mélange. La tomographie optique est une technique d'absorption multiangulaire concernant M mesures d'absorption en ligne (projections) à N angles. Ces $M \times N$ données sont exploitées pour reconstituer le champ d'écoulement bidimensionnel. Des mesures d'absorption sont effectuées sur du méthane en utilisant la ligne 3,39 μm proche de la résonnance d'un laser He–Ne. Des mesures de concentration moyenne sont obtenues pour trois positions en aval du plan d'émission du jet. Des comparaisons avec les résultats antérieurs sur les profils de concentration axiaux et radiaux montrent un bon accord. La sensibilité des résultats au nombre d'angles et de scans est brièvement décrite. Les résultats démontrent la capacité unique de la tomographie optique pour le diagnostic des champs d'écoulement.

OPTISCHE TOMOGRAFIE ZUR UNTERSUCHUNG VON STRÖMUNGSFELDERN

Zusammenfassung—Die optische Tomografie wurde auf einen turbulenten Methan/Luft-Freistrahl angewendet, um die mittlere Methankonzentration im gesamten Mischungsbereich zu bestimmen. Die optische Tomografie ist eine Mehrwinkel-Absorptionsmethode, die darin besteht, daß M Sichtabsorptionslinien (Projektionen) bei N Winkeln gemessen werden. Mit Hilfe dieser $M \times N$ Messungen wird dann das zweidimensionale Strömungsfeld rekonstruiert. Die Absorptionsmessungen an Methan wurden mit der resonanznahen 3,39 μm-Linie eines He–Ne-Lasers durchgeführt. Die mittleren Konzentrationen wurden an drei Positionen stromabwärts von der Austrittsebene des Strahles gemessen. Vergleiche mit den Ergebnissen früherer Experimentatoren für die axialen und radialen mittleren Konzentrationsprofile zeigen gute Übereinstimmung. Ferner wird die Empfindlichkeit der Ergebnisse auf die Anzahl der Linien und Winkel kurz beschrieben. Die Ergebnisse demonstrieren die einzigartigen Möglichkeiten der optischen Tomografie für die Untersuchung von Strömungsfeldern.

ИСПОЛЬЗОВАНИЕ ОПТИЧЕСКОЙ ТОМОГРАФИИ ДЛЯ ДИАГНОСТИКИ ПОЛЯ ТЕЧЕНИЯ

Аннотация — Оптическая томография была применена для случая турбулентного струйного истечения смеси метана с воздухом для определения средней концентрации метана в области смешения. Оптическая томография - это метод измерения поглощения по M визирным линиям (проекциям) в N углах. Затем по данным $M \times N$ измерений строится картина первоначального двумерного поля течения. Измерения проводились на метане с использованием ближней резонансной линии 3,39 мкм гелий–неонового лазера. Средние значения концентраций измерялись в трех положениях за плоскостью истечения струи. Получено хорошее совпадение с результатами работ других авторов для аксиальных и радиальных средних профилей концентрации. Кроме того, дано краткое описание влияния числа углов и сканирований на чувствительность измерений. Полученные результаты демонстрируют возможности оптической томографии для диагностики течений.